Unraveling the Mechanism of a Reversible Photo-Activated Molecular Proton Crane.

ARTICLE *in* THE JOURNAL OF PHYSICAL CHEMISTRY B · OCTOBER 2014

Impact Factor: 3.3 · DOI: 10.1021/jp508911v · Source: PubMed

6 AUTHORS, INCLUDING:

Tibert Hendrik van der Loop
University of Amsterdam
5 PUBLICATIONS **17** CITATIONS
SEE PROFILE

Saeed Amirjalayer
University of Amsterdam
39 PUBLICATIONS **602** CITATIONS
SEE PROFILE

Wybren J Buma
University of Amsterdam
184 PUBLICATIONS **2,463** CITATIONS
SEE PROFILE

Sander Woutersen
University of Amsterdam
103 PUBLICATIONS **4,309** CITATIONS
SEE PROFILE

THE JOURNAL OF PHYSICAL CHEMISTRY B

Article

pubs.acs.org/JPCB

Unraveling the Mechanism of a Reversible Photoactivated Molecular Proton Crane

Tibert H. van der Loop,[†,‡] Freek Ruesink,[†,‡] Saeed Amirjalayer,[†] Hans J. Sanders,[†] Wybren J. Buma,*[,†] and S. Woutersen*[,†]

[†]Van 't Hoff Institute for Molecular Sciences, University of Amsterdam, Science Park 904, 1098 XH Amsterdam, The Netherlands

Supporting Information

ABSTRACT: We study the structural dynamics of the photoactivated molecular proton crane 7-hydroxy-8-(morpholinomethyl)quinoline using femtosecond UV-pump IR-probe spectroscopy. Upon electronic excitation, a proton is transferred from the hydroxy to the amine group located on the rotatable morpholino side group. This morpholino group subsequently delivers the proton to the aromatic quinoline nitrogen by rotation around the C−C bond. Time-resolved vibrational spectroscopy allows us to study this process in unprecedented detail. We find that the transport of the proton involves multiple time scales. Upon photoexcitation, the OH proton is transferred within <300 fs to the morpholino side group. After this, the intramolecular hydrogen bond that locks the crane arm breaks with a time constant of 36 ± 1 ps. Subsequently, the protonated crane arm rotates with a time constant of 334 ± 12 ps to deliver the proton at the quinoline moiety. After the proton crane has returned to its electronic ground state with a time constant 700 ± 22 ps, the proton is transferred back from the quinoline nitrogen to the negatively charged O atom. The time constant of the back rotation is 39.8 ± 0.2 ns, about 200 times slower than the forward proton transfer.

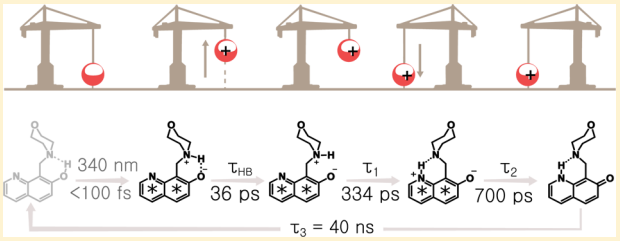

INTRODUCTION

Inspired by biological molecular machines that produce nanoscale motion, and that are at the basis of many fundamental cellular processes, there is an ever-increasing effort to push back the boundaries of device miniaturization, down to the molecular level. This field of nanotechnology involves the concerted efforts of disciplines ranging from biology to chemistry and physics. Key challenges are realizing controlled movements of molecule-sized parts with respect to each other on the molecular length scale to realize targeted tasks. One such task of particular importance is the transportation of mass between two positions under the influence and control of an external stimulus. In recent years a number of impressive achievements have been reached in this respect. Examples include the use of mechanically interlocked architectures such as catenanes[1−3] and rotaxanes[3,4] to induce translational motion such as directed motion along an axle and linear transportation of molecular cargos.

Transport of molecules can also involve pivoting rather than translational motion. Biochemical examples of such pivoting include aromatic side-group rotations involved in the gating of substrate access to the active site in proteins,[5,6] heme pivoting which is believed to act as a substrate selection mechanism,[7] and on a larger scale, the rotation of the legs of the kinesin motor protein.[8,9] To obtain a deeper understanding of such molecular pivoting motions, it is essential to study them in a well-controlled manner, and ideally with a probe that is sensitive to conformational changes at the level of specific covalent bonds. As a first step in this direction, in the present study we employ the architecture of a molecular crane to study pivotal motion, which in this case is used to transport a cargo consisting of a proton. The molecular crane we use for this purpose is 7-hydroxy-8-(morpholinomethyl)quinoline (HMMQ, see Scheme 1). Photoexcitation of the crane increases the acidity of the OH group that releases the proton and the basicity of the group where the proton is delivered. Varma and co-workers were the first to demonstrate the proton-craning behavior of this molecule.[10] The proton crane has been studied previously by steady-state fluorescence, time-resolved fluorescence, and transient absorption spectroscopies

Scheme 1. Different Structures of HMMQ in the Ground State and Electronically Excited State

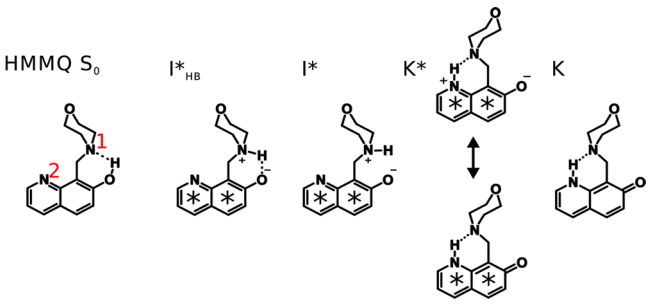

Received: September 3, 2014
Revised: October 15, 2014
Published: October 15, 2014

dx.doi.org/10.1021/jp508911v | J. Phys. Chem. B 2014, 118, 12965−12971

as well as simulations.[10−17] Interestingly, the intermolecular hydrogen-bond breaking that should precede the craning has never been observed. The ground-state retautomerization has also never been observed, as it was thought to occur too fast.[12,13] The experimental techniques employed previously are intrinsically not capable of providing a complete picture of the structural changes that occur during the different steps of the photocycle of the proton crane. Techniques based on emission require that the fluorescence bands of the various intermediate stages of the craning process are different, but in practice it has been found that they are difficult to separate. Furthermore, these techniques are only sensitive to species with a significant fluorescence quantum yield. As a result, "dark" excited-state species can only be studied indirectly, while the return reaction to the initial species that occurs on the ground-state potential-energy surface cannot be studied at all. UV/vis transient-absorption spectroscopy avoids some of these problems, but it is primarily sensitive to changes that occur in the chromophoric part of the crane and much less to those that occur in the other parts. Moreover, it still suffers from the fact that electronic transitions intrinsically probe the entire chromophoric part of the system and are thus not very sensitive to specific local details such as, for example, the making and breaking of hydrogen bonds.

Time-resolved vibrational spectroscopy has emerged as a powerful technique to tackle these issues.[4,18−25] The frequencies and intensities of the bands in a vibrational absorption spectrum provide a direct fingerprint of the structural details of the system, while the bands are generally sufficiently narrow that different species can easily be distinguished. In the present study, we use time-resolved vibrational spectroscopy in combination with UV excitation to read out the operational state of the molecular crane and follow its evolution during its entire photocycle. Apart from determining the time scales at which the different steps in the photocylce occur, we will show evidence that proton transfer in the excited state does (as previously proposed but not directly observed[13]) not lead immediately to rotational Brownian diffusion of the arm of the crane. Rather, the protonated arm needs to be unlocked before it can deliver the proton to the other side of the molecule. Furthermore, we find that the vibrational spectrum in combination with quantum-chemical calculations serves as an excellent probe of the electronic structure of the system and enables us to determine the importance of zwitterionic and neutral mesomeric contributions to its electronic wave function. Finally, we will show that the reverse craning process that occurs after the molecule has returned to its electronic ground state, and that so far has not been accessible to experiment, can be tracked by monitoring the transient vibrational response at long pump−probe delay times.

EXPERIMENTAL AND THEORETICAL DETAILS

The synthesis of HMMQ is described in the Supporting Information. Solutions (30 mM) of HMMQ in CD_3CN (Eurisotop, >99.8% isotopic purity, dried in 3 Å molecular sieve) were prepared resulting in water concentrations of ∼0.5 mM. The water concentration was measured from the intensity of the OH-stretching mode of H_2O in acetonitrile at 3631 cm^{-1}. A calibration line for this mode has been obtained with Karl Fischer titration. Deuterated HMMQ (dHMMQ) samples were prepared by adding a small amount of D_2O (200 mM) to the samples in CD_3CN. The samples with added D_2O were only used for steady-state infrared absorption experiments. The dynamical measurements were all performed on protonated HMMQ. All steady-state FT-IR spectra were measured on a PerkinElmer Spectrum Two spectrometer (resolution 0.5 or 1 cm^{-1}). The UV−vis spectra were obtained with a HP 8453 spectrometer.

Tunable mid-IR pulses were generated using a 35 fs Coherent Legend Elite Ti:sapphire laser with a repetition rate of 1 kHz pumping a commercial OPA with DFG option (Coherent OPerA). Transient spectra were obtained by subtracting unpumped absorption spectra from the pumped absorption spectra, collected using a custom-built 32 pixel mercury cadmium telluride detector coupled to an Oriel MS260i spectrograph. A rotating sample with CaF_2 windows and a 500 μm spacer was placed in the IR focus. To obtain a large temporal window, we used two different pump sources: (1) For the dynamics from subpicosecond up to 2 ns, 340 nm UV pump pulses, tuned to the absorption maximum of HMMQ (see Supporting Information for the UV−vis absorption spectrum of HMMQ), were generated by sum-frequency mixing the fundamental of the Ti:sapphire laser with 560 nm light (obtained by frequency-doubling the signal output of a home-built, BBO-based OPA) in a 0.25 mm BBO crystal with cut angles $\theta = 35°$, $\phi = 90°$. Samples were pumped with a pulse energy of about 2 μJ in a ∼600 μm diameter focus. The delay between the pump and probe was scanned by mechanically adjusting the length of the beam path of the pump beam. The temporal resolution obtained from the fwhm of the cross-correlation of pump and probe pulses was 300 fs. (2) For the dynamics from 10 ns up to 200 ns, we used a pump pulse generated by a Nd:YAG laser (355 nm, pulse length 3 ns) that was electronically synchronized to the Ti:sapphire system.[4] SVD analyses and global fits were performed using Glotaran.[26] The reported fit uncertainties are one standard deviation.

All quantum chemical calculations were performed using the Gaussian09 program package.[27] Geometry optimization and normal-mode analysis were performed using density functional theory (DFT) at the B3LYP cc-pVDZ level.[28−33] Solvent effects were taken into account using the PCM method[34−36] (solvent acetonitrile). Excited-state calculations were carried out for the first excited state within the framework of time-dependent DFT (TDDFT). The vibrational frequencies have been scaled by 0.975.

RESULTS AND DISCUSSION

Figure 1 shows time-resolved vibrational differential absorption spectra of HMMQ in the 1410−1650 (Figure 1b) and 3230−3470 cm^{-1} (Figure 1c) regions after electronic excitation. The same figure displays the steady-state FTIR spectrum of HMMQ (Figure 1a). The time-resolved spectra clearly show that upon electronic excitation HMMQ evolves through several stages. Within the time resolution of the experiment, the spectra show instantaneous bleaching bands in the OH/NH bending and CC stretching region that match nicely with the bands observed in the steady-state spectrum. Concurrently, induced absorption features are observed between 1410 and 1560 cm^{-1}. This spectrum evolves on a time scale of a few hundred picoseconds to a spectrum in which other broad and weak induced-absorption bands become visible between 1410 and 1540 cm^{-1}. The latter spectrum subsequently decays such that at 300 ns it has completely disappeared. The spectrum in the NH stretch region between 3230 and 3470 cm^{-1} shows a qualitatively similar behavior. Under steady-state conditions this part of the

dx.doi.org/10.1021/jp508911v | J. Phys. Chem. B 2014, 118, 12965−12971

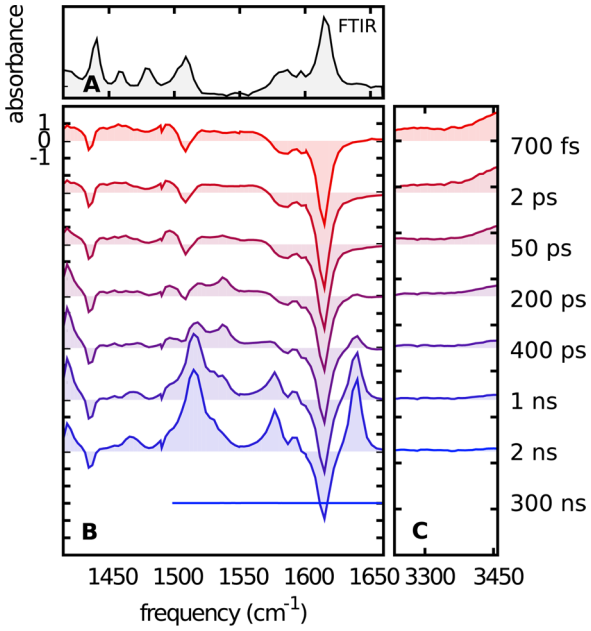

Figure 1. (a) Steady-state absorption of HMMQ. (b) and (c) Transient absorption spectra from 1410 to 1650 cm^{-1} and from 3230 to 3470 cm^{-1} for several delay times after electronic excitation.

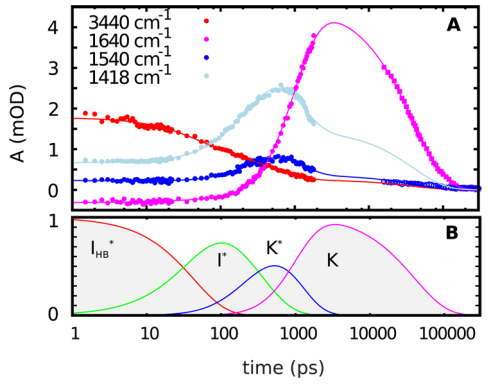

Figure 2. (a) Observed time dependence of the most relevant modes. The lines are a global fit to the data. Between 2 and 10 ns there is a gap because the time ranges of the two experiment methods do not overlap completely. (b) Time evolution of the four-step sequential model.

spectrum does not show any absorbance (the OH-stretch mode absorbs at 2700 cm^{-1} as can been seen in the Supporting Information). Upon excitation an instantaneous broad induced absorption feature is observed that evolves to a small offset value within 2 ns. Interestingly, we find that for pump–probe delays up to 50 ps the spectrum hardly changes in the 6 μm region, while in the 3 μm region much larger changes occur. Below we will argue that the latter observation demonstrates that after the initial proton transfer to the morpholino ring, the arm of the crane still has to overcome a barrier before rotation of the arm can take place.

The spectra in Figure 1 show transient vibrational spectra of the proton crane as it evolves through a number of intermediate structures. To determine the number of spectral components contained in our data set, we performed a singular value decomposition (SVD) analysis.[37,38] For the data between 1410 and 1650 cm^{-1} the first three left and right singular vectors show smooth spectra and delay traces while subsequent components contain only noise (see Supporting Information). We therefore conclude that the data between 1410 and 1650 cm^{-1} can be best described with a three-component system. Figure 2 shows representative delay traces from our data set on a logarithmic time scale. We clearly observe the sequential nature of our data: concurrently with the decrease of the 3440 cm^{-1} band, the bands at 1418 and 1540 cm^{-1} grow in, while subsequently, the decay of the 1418 and 1540 cm^{-1} is accompanied by the rise of the 1640 cm^{-1} band. On the basis of the SVD analysis and the sequential nature of our delay traces, we use a three-component sequential model to make a global fit to our data between 1410 and 1650 cm^{-1}. From this fit we obtain species associated decay rates of $(334 \pm 12\ ps)^{-1}$, $(700 \pm 22\ ps)^{-1}$, and $(39.8 \pm 0.2\ ns)^{-1}$.

The 3230–3470 cm^{-1} frequency region contains a decay component that is faster than that observed in the 1410–1650 cm^{-1} region. Further analysis shows that the time-resolved response in the NH-stretch region cannot be fitted with only the time constants obtained in the fit of the 1410–1650 cm^{-1} data, but that an additional time constant is required. Initial attempts to fit the 3230–3470 cm^{-1} data globally with four exponents were not successful. Apparently, this frequency region is much less sensitive to the structural changes that are causing the changes in the IR spectrum in the 1410–1650 cm^{-1} region. By itself this is not surprising, as the 3230–3470 cm^{-1} region probes the properties of the NH moiety, while the 1410–1650 cm^{-1} region probes the entire molecule. We have therefore fitted the 1410–1650 and 3230–3470 cm^{-1} data globally with the slower three rates kept fixed to the values as obtained from the fit of only the 1410–1650 cm^{-1} data. We then find for the fast decay rate mentioned previously a value of $k_{HB} = 36 \pm 1$ ps. The time-dependent evolution of the normalized concentration of the sequential species is depicted in Figure 2b.

In the following, we will analyze the species associated difference spectra (SADS) that result from these fits and determine the structure that is associated with each of the species, guided by the results of complementary quantum-chemical calculations that include solvent effects. Figures 3a, b, and c show the steady-state FTIR spectrum of HMMQ together with the SADS obtained from the global fit of the 1410–1650 and 3230–3470 cm^{-1} regions. In Figure 3 we also compare the experimental steady-state spectrum and SADS with spectra obtained from DFT calculations. To this purpose we show in panel d the calculated ground-state spectrum of HMMQ and in panel e calculated difference spectra obtained by subtracting the calculated ground-state spectrum from the calculated spectrum of the intermediate species. The accompanying structures are depicted in panel f.

In the electronic ground state, the proton that will be transferred resides on the oxygen atom. Comparison of the measured (Figure 3a) and the predicted (Figure 3d) vibrational absorption spectra shows good agreement, except for the intensities of the G3 and G4 bands. Inspection of the modes associated with the various bands reveals that band G2 is an aliphatic CH-bend vibration, G1 an aliphatic aromatic CH-bend combination vibration with OH-bend character, while G4, G5, and G6 are varying mixtures of CC-ring stretch vibrations and the OH-bend vibration with G4 having the smallest OH-bend contribution. The assignment of the vibrations with OH-bending character by DFT is supported by the observation that G2 and G4 are least affected by hydrogen/deuterium exchange

dx.doi.org/10.1021/jp508911v | J. Phys. Chem. B 2014, 118, 12965–12971

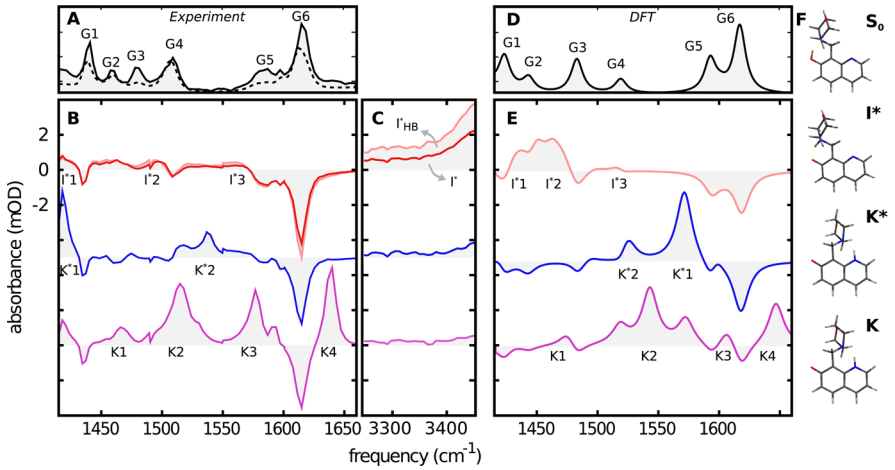

Figure 3. (a) FTIR spectrum of HMMQ (solid) and dHMMQ (dashed) in acetonitrile. SADS from a global fit between 1410 and 1650 cm^{-1} (b) and 3230−3470 cm^{-1} (c). These spectra belong to the sequential steps that are involved in the photocycle. (d) Calculated ground-state infrared spectrum of HMMQ. (e) Calculated difference spectra of the intermediate species. The frequencies have been scaled by 0.975. The associated structures are depicted on the right. (f) The molecular structures associated with the calculated spectra (see also Scheme 1).

when comparing the steady-state spectra of HMMQ with dHMMQ (Figure 3a).

Species I* grows in within the time resolution of the experiment and decays monoexponentially with a lifetime of 334 ± 12 ps. As will be shown below, in this species the proton is transferred from the hydroxy to the N1 group (see Scheme 1). Inspection of the associated SADS in Figure 3 shows clear bleaches at positions that coincide with the ground-state ring vibrations G1, G3, G4, G5, and G6. Importantly, we find that at the position of G2 no bleach is observed. Apparently, excitation does not lead to appreciable changes in the electronic structure of the part that is associated with these vibrations. This is completely in line with our assignment of G2 to aliphatic C−H vibrations on the morpholino side group since this group is not part of the conjugated ring structure. Analogously, the bleach in the ring and OH-bending vibrations confirms that we have excited the conjugated ring structure and that the OH proton has been effected by the excitation. The induced absorptions in the experimental spectra are relatively weak and broad, but compare very well with the induced absorption features I*1 and I*3 predicted in the calculated difference spectra. Comparison of the ground- and excited-state geometries as obtained from the DFT optimizations in which solvent effects were included reveals that upon excitation the OH bond length increases from 1.01 to 1.59 Å, while the distance from the OH proton to N1 decreases from 1.68 to 1.07 Å. This observation confirms that the proton is indeed transferred from the hydroxyl group to N1. At the same time, it should be noted that the same calculations indicate that the solvent plays a decisive role in the proton transfer process, since calculations that do not include solvent effects come up with quite a different picture. In these calculations the OH-bond length increases only 0.01 Å, while the intramolecular hydrogen bond between OH and N1 decreases from 1.74 to 1.58 Å. The calculations thus show that electronic excitation of the isolated molecule in first instance does not lead to a full proton transfer from the oxygen to the nitrogen atom, but rather to an increased bonding of the proton with the nitrogen atom. The importance of solvent interactions is confirmed by similar UV-IR pump−probe experiments that we have performed in an apolar solvent (*n*-hexane) in which we find that proton transfer is completely absent (see Supporting Information). We thus conclude that in our experiments in acetonitrile a full proton transfer can be achieved because interactions of the excited species with the solvent are able to stabilize the proton-transferred species. The instantaneous rise of I* implies that this proton transfer occurs faster than our experimental time resolution (300 fs). Such a high rate is in good agreement with experiments on other photoacids which show ultrafast subpicosecond excited-state intramolecular proton transfer (ESIPT) through direct contact of the proton donor and acceptor.[39−43]

In the NH-stretch region we observe a broad induced-absorption feature from the NH stretch vibration that appears within the experimental time resolution. This signal shows an initial decay time constant of 36 ± 1 ps. The observation that in the 1410−1650 cm^{-1} region the SADS changes only slightly when compared to the SADS of the next step indicates that the process that is associated with this time constant does not involve the aromatic backbone or morpholino ring, whereas comparison of the SADS labeled I^*_{HB} and I* in Figure 3c shows that the nature of the NH-stretch vibration changes significantly: there is a decrease of the NH-stretch absorption cross section and a blue shift of the band. Both characteristics are typical of NH-stretch modes that initially are hydrogen-bonded but become non-hydrogen-bonded or more weakly hydrogen-bonded.[44,45] We therefore conclude that the time constant of 36 ± 1 ps is associated with the intramolecular hydrogen-bond breaking required for the rotation of the morpholine ring. A number of alternative explanations that might in the first instance come to mind can be excluded. First, diffusion reorientation of the molecule can be excluded because the measurements have been performed under magic angle conditions. Another explanation for the fast decay might be intramolecular vibrational relaxation (IVR), but the observed rate of 36 ± 1 ps^{-1} is too slow for IVR.[46,47] More important, however, is that in that case this lifetime would also be expected to be observed in the low-frequency range. The observed lifetime τ_{HB} is in good agreement with hydrogen bond lifetimes in similar systems.[48]

After breaking of the NH···O hydrogen bond between the morpholino ring and the aromatic oxygen, a new species K* is formed with a time constant of 334 ± 12 ps. Previous fluorescence and transient-absorption experiments associated this species with the excited-state isomer that is generated by

dx.doi.org/10.1021/jp508911v | J. Phys. Chem. B 2014, 118, 12965−12971

Brownian rotation of the morpholino group and subsequent transfer of the proton from the morpholino group to the quinolinic nitrogen atom. An important issue that cannot be addressed by such studies, however, concerns the finer details of the spatial and electronic structure of this species. Here we will show that the C−O stretch vibration can be employed as a sensitive probe for determining this structure. Comparison of the SADS of K* with the calculated difference spectrum for this species shows overall good agreement. The only notable exceptions are a strong induced absorption band found in the experimental spectrum at 1420 cm^{-1} that is not found in the calculated spectrum, and vice versa a strong induced absorption band at 1570 cm^{-1} in the calculated spectrum that is not observed in the experimental spectrum. The calculations reveal that this 1570 cm^{-1} K*1 band arises from the carbonyl stretch vibration, which means that the frequency of this mode is calculated significantly higher than experimentally observed. The large reduction of the carbonyl-stretch frequency implies that its double-bond character is strongly reduced, i.e., the keto form that so far has been associated with this species has a considerable contribution from mesomeric structures in which the CO bond has single-bond character. In the latter case the C−O frequency is typically found at around 1300 cm^{-1}.[49−51] It is known that DFT calculations tend to drastically overestimate the C−O stretch vibrations when the electronic structure is described by a combination of mesomeric conformations. For example, the phenolate ion shows a red shift of around 100 cm^{-1} in the calculated C−O vibration compared to the experimental value.[52] The observation of a C−O vibration at 1420 cm^{-1} indicates that the wave function of the excited state contains—in valence bond terms—a large fraction of the zwitterionic form.

After the formation of K*, the last species K grows in with a rate of $(700 \pm 22\ ps)^{-1}$ and decays with a rate of $(39.8 \pm 0.2\ ns)^{-1}$. Figure 3 shows that the SADS of this species is in excellent agreement with the spectrum predicted for the ground state of the keto form (see Scheme 1). Experiments based on detection of the fluorescence of the system clearly cannot detect this species, and it has therefore not been reported before in these experiments[13,53] One of the features that characterizes this spectrum is the shift to higher frequency of the mixed CC ring stretch/NH bend vibration (band K4), and the strong induced absorption of band K2 and K3 associated with the symmetric and anti-symmetric combination modes of the C−O stretch and N−H bend. The shift to higher frequency indicates that in state K the carbonyl group has more C═O character than K* (K2 and K3 being the symmetric and the antisymmetric CO-stretch + NH-bend combination modes). Experimental confirmation that these features are expected to occur in the IR spectrum of the ground state of the keto form is obtained from the IR spectrum of 7-hydroxyquinolinium chloride (see Supporting Information), which displays the same features at approximately the same frequencies as observed in the transient spectrum for long time delays. We thus conclude that the decay of species K* involves the return of the molecule in the keto form to its electronic ground state. The decay of the transient difference spectrum then indicates that this ground-state species undergoes proton back transfer to yield the original enol form of the molecule (without the observation of any intermediate state). Remarkably, we thus find that the reverse craning process is more than 2 orders of magnitude slower than the first craning step. Assuming that the rotational diffusion of the crane arm is not affected by electronic excitation, we can exclude diffusion as a possible reason for the different craning rates. Instead, we propose that the return craning rate in the ground state is limited by the intramolecular proton transfer process from N2 to N1. Consideration of the pK_a values of N1 and N2 in the ground state shows that they are only slightly different (7.38 and 5.4, respectively).[54,55] It is therefore not unreasonable to assume that there is an energy barrier for the proton transfer step between N1 and N2 in the ground state. In line with this idea we find that for the first (excited-state) proton transfer step, which has been concluded to occur without barrier, the difference between the excited state pK_a values of O (−3.1)[56] and N1 (7.38)[55] is significantly larger (10.48).

CONCLUSION

We have reported on the operation of a photoactivated molecular proton crane using ultrafast UV-pump IR-probe spectroscopy. The time-resolved infrared spectra revealed sequential dynamics involving five steps through which the proton crane operates. The structures of the intermediate states were identified by comparing species-associated infrared difference spectra with both excited-state and ground-state DFT calculations. The following steps were identified: intramolecular proton transfer (loading of the crane arm), intramolecular hydrogen-bond breaking (unlocking of the crane arm), Brownian rotation of the protonated morpholino side group (transporting the load), excited-state relaxation, and finally ground-state retautomerization (transporting the load back to its initial position) with respective time constants of <300 fs, 36 ± 1 ps, 334 ± 12 ps, 700 ± 22 ps, and 39 ± 0.2 ns. The observed frequency of the C−O vibration confirms the mesomeric character of the electronically excited state. In the transient vibrational spectra, we directly observe the intramolecular hydrogen-bond breaking that precedes the rotational diffusion of the molecular crane arm, as well as the proton back transfer which occurs in the electronic ground state. These results demonstrate that time-resolved infrared spectroscopy is an effective means to probe the pivoting motion of a molecular machine, revealing mechanistic details that cannot be observed using other techniques.

ASSOCIATED CONTENT

Supporting Information

Synthesis procedure; UV−vis and IR absorption spectrum of HMMQ; graphical representation of the SVD analysis on the time-resolved difference spectra in the 1410−1650 cm^{-1} region; comparison of species K with a model compound 7-HQ; difference spectrum of HMMQ in *n*-hexane 1700 ps after electronic excitation. This material is available free of charge via the Internet at http://pubs.acs.org.

AUTHOR INFORMATION

Corresponding Authors

*E-mail: W.J.Buma@uva.nl.
*E-mail: S.Woutersen@uva.nl.

Author Contributions

‡T.H.L. and F.R. contributed equally to this work.

Notes

The authors declare no competing financial interest.

■ ACKNOWLEDGMENTS

The authors thank Stichting voor Fundementeel Onderzoek der Materie (FOM) for financial support.

■ REFERENCES

(1) Zhu, Z.; Fahrenbach, A. C.; Li, H.; Barnes, J. C.; Liu, Z.; Dyar, S. M.; Zhang, H.; Lei, J.; Carmieli, R.; Sarjeant, A. A.; et al. Controlling Switching in Bistable [2]Catenanes by Combining Donor−Acceptor and Radical−Radical Interactions. *J. Am. Chem. Soc.* **2012**, *134*, 11709−11720.

(2) Black, S. P.; Stefankiewicz, A. R.; Smulders, M. M. J.; Sattler, D.; Schalley, C. A.; Nitschke, J. R.; Sanders, J. K. M. Generation of a Dynamic System of Three-Dimensional Tetrahedral Polycatenanes. *Angew. Chem., Int. Ed.* **2013**, *52*, 5749−5752.

(3) Kay, E.; Leigh, D.; Zerbetto, F. Synthetic Molecular Motors and Mechanical Machines. *Angew. Chem., Int. Ed.* **2007**, *46*, 72−191.

(4) Panman, M. R.; Bodis, P.; Shaw, D. J.; Bakker, B. H.; Newton, A. C.; Kay, E. R.; Brouwer, A. M.; Buma, W. J.; Leigh, D. A.; Woutersen, S. Operation Mechanism of a Molecular Machine Revealed Using Time-Resolved Vibrational Spectroscopy. *Science* **2010**, *328*, 1255−1258.

(5) Zhou, H.-X.; Wlodek, S. T.; McCammon, J. A. Conformation Gating as a Mechanism for Enzyme Specificity. *Proc. Natl. Acad. Sci. U. S. A.* **1998**, *95*, 9280−9283.

(6) Javelle, A.; Lupo, D.; Ripoche, P.; Fulford, T.; Merrick, M.; Winkler, F. K. Substrate Binding, Deprotonation, and Selectivity at the Periplasmic Entrance of the Escherichia Coli Ammonia Channel AmtB. *Proc. Natl. Acad. Sci. U.S.A.* **2008**, *105*, 5040−5045.

(7) Ma, X.; Sayed, N.; Beuve, A.; van den Akker, F. NO and CO Differentially Activate Soluble Guanylyl Cyclase via a Heme Pivot-Bend Mechanism. *EMBO J.* **2007**, *26*, 578−588.

(8) Vale, R. D. The Molecular Motor Toolbox for Intracellular Transport. *Cell* **2003**, *112*, 467−480.

(9) Shiroguchi, K.; Kinosita, K. Myosin V Walks by Lever Action and Brownian Motion. *Science* **2007**, *316*, 1208−1212.

(10) Jalink, C. J.; van Ingen, W. M.; Huizer, A. H.; Varma, C. A. G. O. Prospects for Using Photoinduced Intramolecular Proton Transfer To Study the Dynamics of Conformational Changes in Flexible Molecular Chains. *J. Chem. Soc., Faraday Trans.* **1991**, *87*, 1103−1108.

(11) Jalink, C. J.; Huizer, A. H.; Varma, C. A. G. O. Rotational Brownian Motion of the Proton Crane Operating in a Photoinduced Long-Distance Intramolecular Proton Transfer. *J. Chem. Soc., Faraday Trans.* **1992**, *88*, 1643−1651.

(12) Jalink, C. J.; Huizer, A. H.; Varma, C. A. G. O. Rate-Limiting Action of a Proton Crane in Long-Range Intramolecular Proton Transfer. *J. Chem. Soc., Faraday Trans.* **1992**, *88*, 2655−2659.

(13) de Bekker, E. J. A.; Pugzlys, A.; Varma, C. A. G. O. Elementary Processes in Photoinduced Proton Transfers in 2-Hydroxy-1-(*N*-morpholinomethyl)naphthalene and 7-Hydroxy-8-(*N*-morpholinomethyl)quinoline in Liquid Solutions. *J. Phys. Chem. A* **2000**, *105*, 399−409.

(14) de Bekker, E. J. A.; Geerlings, J. D.; Varma, C. A. G. O. Mechanism of a Photoinduced Solvent-Assisted Transfer of a Proton to a Specified Remote Target. *J. Phys. Chem. A* **2000**, *104*, 5916−5927.

(15) Sobolewski, A. L. Reversible Molecular Switch Driven by Excited-State Hydrogen Transfer. *Phys. Chem. Chem. Phys.* **2008**, *10*, 1243−1247.

(16) Rode, M. F.; Sobolewski, A. L. Effect of Chemical Substituents on the Energetical Landscape of a Molecular Photoswitch: An ab Initio Study. *J. Phys. Chem. A* **2010**, *114*, 11879−11889.

(17) Vetokhina, V.; Nowacki, J.; Pietrzak, M.; Rode, M. F.; Sobolewski, A. L.; Waluk, J.; Herbich, J. 7-Hydroxyquinoline-8-carbaldehydes. 2. Prototropic Equilibria. *J. Phys. Chem. A* **2013**, *117*, 9147−9155.

(18) Heyne, K.; Mohammed, O. F.; Usman, A.; Dreyer, J.; Nibbering, E. T. J.; Cusanovich, M. A. Structural Evolution of the Chromophore in the Primary Stages of Trans/Cis Isomerization in Photoactive Yellow Protein. *J. Am. Chem. Soc.* **2005**, *127*, 18100−18106.

(19) Stoner-Ma, D.; Jaye, A. A.; Ronayne, K. L.; Nappa, J.; Meech, S. R.; Tonge, P. J. An Alternate Proton Acceptor for Excited-State Proton Transfer in Green Fluorescent Protein: Rewiring GFP. *J. Am. Chem. Soc.* **2008**, *130*, 1227−1235.

(20) Brust, R.; Lukacs, A.; Haigney, A.; Addison, K.; Gil, A.; Towrie, M.; Clark, I. P.; Greetham, G. M.; Tonge, P. J.; Meech, S. R. Proteins in Action: Femtosecond to Millisecond Structural Dynamics of a Photoactive Flavoprotein. *J. Am. Chem. Soc.* **2013**, *135*, 16168−16174.

(21) Reichardt, C.; Schroeder, J.; Vöhringer, P.; Schwarzer, D. Unravelling the Ultrafast Photodecomposition Mechanism of Dibenzoyl Peroxide in Solution by Time-Resolved IR Spectroscopy. *Phys. Chem. Chem. Phys.* **2008**, *10*, 1662−1668.

(22) Hare, P. M.; Middleton, C. T.; Mertel, K. I.; Herbert, J. M.; Kohler, B. Time-Resolved Infrared Spectroscopy of the Lowest Triplet State of Thymine and Thymidine. *Chem. Phys.* **2008**, *347*, 383−392.

(23) To, T. T.; Heilweil, E. J.; Duke, C. B.; Ruddick, K. R.; Webster, C. E.; Burkey, T. J. Development of Ultrafast Photochromic Organometallics and Photoinduced Linkage Isomerization of Arene Chromium Carbonyl Derivatives. *J. Phys. Chem. A* **2009**, *113*, 2666−2676.

(24) Asplund, M. C.; Snee, P. T.; Yeston, J. S.; Wilkens, M. J.; Payne, C. K.; Yang, H.; Kotz, K. T.; Frei, H.; Bergman, R. G.; Harris, C. B. Ultrafast UV Pump/IR Probe Studies of C−H Activation in Linear, Cyclic, and Aryl Hydrocarbons. *J. Am. Chem. Soc.* **2002**, *124*, 10605−10612.

(25) Zhang, W.; Lan, Z.; Sun, Z.; Gaffney, K. J. Resolving Photo-Induced Twisted Intramolecular Charge Transfer with Vibrational Anisotropy and TDDFT. *J. Phys. Chem. B* **2012**, *116*, 11527−11536.

(26) Snellenburg, J. J.; Laptenok, S.; Seger, R.; Mullen, K. M.; van Stokkum, I. H. M. Glotaran: A Java-Based Graphical User Interface for the R Package TIMP. *J. Stat. Soft.* **2012**, *49*, 1−22.

(27) Frisch, M. J.; Trucks, G. W.; Schlegel, H. B.; Scuseria, G. E.; Robb, M. A.; Cheeseman, J. R.; Scalmani, G.; Barone, V.; Mennucci, B.; Petersson, G. A.; et al. *Gaussian 09*, revision D.01; Gaussian, Inc.: Wallingford CT, 2009.

(28) Becke, A. D. Density-Functional Exchange-Energy Approximation with Correct Asymptotic Behavior. *Phys. Rev. A* **1988**, *38*, 3098−3100.

(29) Lee, C.; Yang, W.; Parr, R. G. Development of the Colle-Salvetti Correlation-Energy Formula into a Functional of the Electron Density. *Phys. Rev. B* **1988**, *37*, 785−789.

(30) Stephens, P. J.; Devlin, F. J.; Chabalowski, C. F.; Frisch, M. J. Ab Initio Calculation of Vibrational Absorption and Circular Dichroism Spectra Using Density Functional Force Fields. *J. Phys. Chem.* **1994**, *98*, 11623−11627.

(31) Figgen, D.; Rauhut, G.; Dolg, M.; Stoll, H. Energy-Consistent Pseudopotentials for Group 11 and 12 Atoms: Adjustment to Multi-configuration Dirac−Hartree−Fock Data. *Chem. Phys.* **2005**, *311*, 227−244.

(32) Peterson, K. A.; Puzzarini, C. Systematically Convergent Basis Sets for Transition Metals. II. Pseudopotential-Based Correlation Consistent Basis Sets for the Group 11 (Cu, Ag, Au) and 12 (Zn, Cd, Hg) Elements. *Theor. Chem. Acc.* **2005**, *114*, 283−296.

(33) Wilson, A. K.; Woon, D. E.; Peterson, K. A.; Dunning, T. H. Gaussian Basis Sets for Use in Correlated Molecular Calculations. IX. The Atoms Gallium through Krypton. *J. Chem. Phys.* **1999**, *110*, 7667−7676.

(34) Miertus, S.; Scrocco, E.; Tomasi, J. Electrostatic Interaction of a Solute with a Continuum. A Direct Utilizaion of ab Initio Molecular Potentials for the Prevision of Solvent Effects. *Chem. Phys.* **1981**, *55*, 117−129.

(35) Miertus, S.; Tomasi, J. Approximate Evaluations of the Electrostatic Free Energy and Internal Energy Changes in Solution Processes. *Chem. Phys.* **1982**, *65*, 239−245.

(36) Tomasi, J.; Mennucci, B.; Cammi, R. Quantum Mechanical Continuum Solvation Models. *Chem. Rev.* **2005**, *105*, 2999−3094.

(37) Eckart, C.; Young, G. The Approximation of One Matrix by Another of Lower Rank. *Psychometrika* **1936**, *1*, 211−218.

(38) Panman, M. R.; Bodis, P.; Shaw, D. J.; Bakker, B. H.; Newton, A. C.; Kay, E. R.; Leigh, D. A.; Buma, W. J.; Brouwer, A. M.; Woutersen, S. Time-Resolved Vibrational Spectroscopy of a Molecular Shuttle. *Phys. Chem. Chem. Phys.* **2012**, *14*, 1865−1875.
(39) Luber, S.; Adamczyk, K.; Nibbering, E. T. J.; Batista, V. S. Photoinduced Proton Coupled Electron Transfer in 2-(2′-Hydroxyphenyl)-Benzothiazole. *J. Phys. Chem. A* **2013**, *117*, 5269−5279.
(40) Chevalier, K.; Wolf, M. M. N.; Funk, A.; Andres, M.; Gerhards, M.; Diller, R.; Transient, I. R. Spectroscopy and ab Initio Calculations on ESIPT in 3-Hydroxyflavone Solvated in Acetonitrile. *Phys. Chem. Chem. Phys.* **2012**, *14*, 15007−15020.
(41) Schriever, C.; Barbatti, M.; Stock, K.; Aquino, A. J.; Tunega, D.; Lochbrunner, S.; Riedle, E.; de Vivie-Riedle, R.; Lischka, H. The Interplay of Skeletal Deformations and Ultrafast Excited-State Intramolecular Proton Transfer: Experimental and Theoretical Investigation of 10-Hydroxybenzo[h]quinoline. *Chem. Phys.* **2008**, *347*, 446−461.
(42) Dwyer, J. R.; Dreyer, J.; Nibbering, E. T.; Elsaesser, T. Ultrafast Dynamics of Vibrational N−H Stretching Excitations in the 7-Azaindole Dimer. *Chem. Phys. Lett.* **2006**, *432*, 146−151.
(43) Elsaesser, T.; Kaiser, W. Visible and Infrared Spectroscopy of Intramolecular Proton Transfer Using Picosecond Laser Pulses. *Chem. Phys. Lett.* **1986**, *128*, 231−237.
(44) Skinner, J. L.; Auer, B. M.; Lin, Y.-S. *Advances in Chemical Physics*; John Wiley & Sons, Inc.: New York, 2008; pp 59−103.
(45) Nibbering, E.; Dreyer, J.; Kühn, O.; Bredenbeck, J.; Hamm, P.; Elsaesser, T. In *Chemical Physics*; Kühn, O., Wöste, L., Eds.; Springer: Berlin, Heidelberg, 2007; Vol. *87*, pp 619−687.
(46) Kayano, M.; Ebata, T.; Yamada, Y.; Mikami, N. Picosecond IR−UV Pump−Probe Spectroscopic Study of the Dynamics of the Vibrational Relaxation of Jet-Cooled Phenol. II. Intracluster Vibrational Energy Redistribution of the OH Stretching Vibration of Hydrogen-Bonded Clusters. *J. Chem. Phys.* **2004**, *120*, 7410−7417.
(47) Yamada, Y.; Mikami, N.; Ebata, T. Relaxation Dynamics of NH Stretching Vibrations of 2-Aminopyridine and Its Dimer in a Supersonic Beam. *Proc. Natl. Acad. Sci. U.S.A.* **2008**, *105*, 12690−12695.
(48) Zheng, J.; Fayer, M. D. Hydrogen Bond Lifetimes and Energetics for Solute/Solvent Complexes Studied with 2D-IR Vibrational Echo Spectroscopy. *J. Am. Chem. Soc.* **2007**, *129*, 4328−4335.
(49) Miyazaki, M.; Kawanishi, A.; Nielsen, I.; Alata, I.; Ishiuchi, S.-i.; Dedonder, C.; Jouvet, C.; Fujii, M. Ground State Proton Transfer in Phenol−$(NH_3)_n$ ($n \geq 11$) Clusters Studied by Mid-IR Spectroscopy in 3−10 μm Range. *J. Phys. Chem. A* **2013**, *117*, 1522−1530.
(50) Milko, P.; Roithová, J.; Tsierkezos, N.; Schröder, D. The C−O Stretch as an Unprecedently Large Spectral Marker for the Electron Transfer between Copper(II) and a Phenolate Anion. *J. Am. Chem. Soc.* **2008**, *130*, 7186−7187.
(51) Mukherjee, A.; McGlashen, M. L.; Spiro, T. G. Ultraviolet Resonance Raman Spectroscopy and General Valence Force Field Analysis of Phenolate and Phenoxyl Radical. *J. Phys. Chem.* **1995**, *99*, 4912−4917.
(52) Suter, H. U.; Nonella, M. A Quantum Chemical Investigation of the C−O Bond Length and Stretching Mode of the Phenolate Anion. *J. Phys. Chem. A* **1998**, *102*, 10128−10133.
(53) A tentative observation of the species was reported in transient absorption experiments, but these experiments were far from conclusive.
(54) Nakagawa, T.; Kohtani, S.; Itoh, M. Picosecond Fluorescence and Two-Step LIF Studies of the Excited-State Proton Transfer in Methanol Solutions of 7-Hydroxyquinoline and Methyl-Substituted 7-Hydroxyquinolines. *J. Am. Chem. Soc.* **1995**, *117*, 7952−7957.
(55) Mirgorodskaya, A.; Valeeva, F.; Kudryavtseva, L.; Vylegzhanina, N.; Zuev, Y. Reaction of Carboxylic Acid Esters with Phenolates in Oil-in-Water Microemulsions Based on Cetyltrimethylammonium Bromide. *Russ. J. Gen. Chem.* **2006**, *76*, 590−595.
(56) Han, K.-L.; Zhao, G.-J. In *Hydrogen Bonding and Transfer in the Excited State*; Han, K.-L., Zhao, G.-J., Eds.; Wiley: New York, 2010; Vol. *I*.